Application of anisotropy of magnetic susceptibility (AMS) fabrics to determine the kinematics of active tectonics: Examples from the Betic Cordillera, Spain and the northern Apennines, Italy.

David J. Anastasio[1], Frank J. Pazzaglia[1], Josep M. Parés[2], Kenneth P. Kodama[1], Claudio Berti[3], James A. Fisher[1], Alessandro Montanari[4], Lorraine K. Carnes[5]

[1] Department of Earth and Environmental Sciences, Lehigh University, Bethlehem, PA, 18015-3001, United States
[2] Geochronology, Centro Nacional de Investigación de la Evolución Humana (CENIEH) Burgos, 09002, Spain
[3] Idaho Geological Survey, Moscow, ID, 83844-3014, United States
[4] Osservatorio Geologico di Coldigioco, Apiro MC, 62021, Italy
[5] Arizona State University, Tempe, AZ, 85281, United States

Correspondence to: David J. Anastasio (dja2@lehigh.edu)

Abstract: The anisotropy of magnetic susceptibility (AMS) technique provides an effective way to measure fabrics and in the process, interpret the kinematics of actively deforming orogens. We collected rock fabric data of alluvial fan sediments surrounding the Sierra Nevada massif, Spain, and a broader range of Cenozoic sediments and rocks across the northern Apennine foreland, Italy, to explore the deformation fabrics that contribute to the ongoing discussions of orogenic kinematics. Sierra Nevada is a regional massif in the hinterland of the Betic Cordillera. We recovered nearly identical kinematics regardless of specimen magnetic minerology, structural position, crustal depth, or time. The principal elongation axes are NE-SW in agreement with mineral lineations, regional GPS geodesy, and seismicity results. The axes trends are consistent with the convergence history of the Africa-Eurasia plate boundary. In Italy, we measured AMS fabrics of specimens collected along a NE-SW corridor spanning the transition from crustal shortening to extension in the northern Apennines. Samples have AMS fabrics compatible only with shortening in the Apennine wedge and have locked in penetrative contractional fabrics, even for those samples that were translated into the actively extending domain. In both regions we found that specimens have a low degree of anisotropy and oblate susceptibility ellipsoids that are consistent with tectonic deformation superposed on compaction fabrics. Collectively, these studies demonstrate the novel ways that AMS can be combined with structural, seismic, and GPS geodetic data to resolve orogenic kinematics in space and time.

1 Introduction

A number of *circum*-Mediterranean orogens are associated with rapid slab rollback, resulting in paired compressional and extensional domains in the orogenic wedge of the retreating upper plate (Elter, 1975, Carminati and Doglioni, 2012). Examples include, the Calabria Arc-Tyrrhenian Sea (Beccaluva et al. 1985; Milia et al 2009), the Hellenic Arc-Aegean Sea (Pichon and Angelier 1979; Papazachos et al. 2000), and the Gibraltar Arc-Alboran Sea (Lonergan and White 1997; Platt et al. 2006; Fernández-Ibáñez and Soto 2008). Along these tectonic boundaries, the temporal and spatial relationship between thrust belt contraction, wedge-top basin evolution,

hinterland extension, and orogenic uplift are the subjects of continuing controversy.

Finite and incremental strain data provide deformation history and fabric distribution information for kinematic studies of folds, faults, and orogens (e.g., Cloos, 1947; Ramsay and Huber, 1984; Fischer et al., 1992). However, in orogenic forelands where deformation occurs at shallow depths and low temperatures, ductile penetrative deformation features may be absent and brittle structures may be sparse. Anisotropy of magnetic susceptibility (AMS) results offers an alternative proxy for grain preferred orientation, and hence rock strain, to determine the tectonic fabric in these orogens where other deformation markers are not available (Borradaile and Jackson, 2004; 2010; Borradaile and Henry, 1997; Averbuch et al., 1992; Pares, 2004). In general, comparative studies from siliciclastic rocks show good agreement between both the relative magnitude and orientation of penetrative rock strain determined by traditional geometric methods and AMS principal axes, however, in specimens dominated by diamagnetic mineral abundance, the AMS axes orientation, and not necessarily their magnitude, correlates to the rock strain. (e.g., Latta and Anastasio, 2007; Burneister et al., 2009). In this paper, we show how AMS can extend the temporal reach of GPS geodesy back in time in orogenic studies of the Betic Cordillera, Spain and in the northern Apennines, Italy (e.g., Mattei et al., 2004; Fig. 1).

2 Kinematic Studies For Active Tectonic Research

Sedimentary rocks acquire a primary depositional fabric, which is bedding-parallel. It is measurable with the AMS technique and is further enhanced and modified during burial, compaction, and water loss (e.g., Tarling and Hrouda, 1993; Schwehr et al., 2006). Even unconsolidated rocks record a magnetic fabric that can potentially provide a kinematic record (Mattei et al., 1997; Porreca and Mattei, 2012). The sensitivity of AMS allows its use as a paleogeodetic tool in tectonic studies. Kinematics allow for an assessment of rheology and strain history that are necessary prerequisites for understanding geodynamics, incrementally balancing cross sections, or in paleogeographic reconstructions. We sampled both consolidated sedimentary rocks and unconsolidated sediments in the Betic Cordillera, Spain and northeastern Apennine ranges, Italy for AMS analysis. The Betics field sampling was designed to test AMS recovery from unburied and unconsolidated sediments around the Sierra Nevada massif. Here, oriented samples were collected from sites around the Sierra Nevada massif in Plio-Pleistocene terrestrial, siliciclastic deposits (Table A1). The Apennines field sampling was designed to measure the rotation of strain across the foreland as sampling sites passes from the actively shortening part of the orogenic wedge near the trench to the actively extending regime further to the southwest. Here, oriented samples were collected from sites along a NE-SW oriented corridor inclusive of Cenozoic (Table A1) marine and fluvial siliciclastics, marls, and carbonate rocks, and unconsolidated Pleistocene fluvial sediments.

3 The AMS Method

The AMS ellipsoid is defined by the principal axes (k_1-maximum, k_2-intermediate, k_3-minimum) of a specimen. It can be represented by a second-rank tensor that characterizes a material's magnetization response to an applied magnetic field (e.g., Borradaile and Tarling, 1981; Tarling and Hrouda, 1993). The orientation and relative length of the principal anisotropy axes of a specimen are controlled by the preferred alignment of the anisotropy axes of the

individual magnetic particles in the specimen and the degree of the individual particle's anisotropy. The anisotropy of individual magnetic grains is controlled by their crystallography and grain shape (Tarling and Hrouda, 1993). For magnetite grains, the anisotropy is controlled by grain shape, whereas for hematite and phyllosilicate particles the anisotropy can be controlled by a grain's crystallography, which, in turn, controls their shape. This does not preclude the possibility of the mutual orientation of different particles (e.g. Housen et al., 1993; Weil and Yonkers 2009) or the preferential alignment of iron-bearing inclusions within the particles (e.g. Biedermann, 2018; Borradaile and Werner, 1994; Borradaile and Lagroix, 2000; Martín-Hernandez and Hirt; Parés and van der Pluijm, 2002) controls the AMS.

Natural processes such as current deposition, lithification, and tectonic deformation all contribute to a specimen's AMS. In deformed rocks, it was shown that the principal susceptibility axis (k_1) orientation is typically parallel to the strain long axis and orthogonal to the tectonic shortening direction, whereas the shortest axis (k_3), is orthogonal to bedding in orientation (e.g., Kligfield et al., 1982; Hrouda, 1982), regardless of whether the individual particle anisotropy is controlled by crystallography or shape.

The sedimentary rocks and deposits in this study contain enough phyllosilicate minerals to be excellent specimens for AMS studies because of the presence of oblate mineral grains which adjust readily to deposition, lithification, and any subsequent deformation. As grains reorient in response to depositional or tectonic processes, the magnetic fabric will continuously adjust (Parés and van der Pluijm, 2002). Deposition from currents in alluvial fans or rivers like the examples discussed here, will cause preferred grain alignment. Because the intermediate and maximum AMS axes of platy grains, such as phyllosilicates, are nearly equal in magnitude they will be randomly oriented within the bedding plane, with the minimum axes orthogonal to bedding. In mudstones and fine grained sandstones, where both paramagnetism and ferromagnetism contributions were quantified, paramagnetic mineral grains typically dominate the AMS signal (e.g. Martin-Hernández and Hirt, 2001) because of the shape anisotropy of clay minerals, although very fine magnetic particles attached to the clay fabric might also contribute (Kodama and Sun, 1992).

4 Example I: Sierra Nevada Massif, Spain

4.1 Geologic Setting of Sierra Nevada Massif

The Sierra Nevada massif is part of the Betic Cordillera-Rif-Tell orogens that extend along the European-African plate boundary from the southern Iberian peninsula to northern Africa. These orogens were formed by slab rollback and western migration of the Gibraltar Arc throughout the Neogene (Rosenbaum et al., 2002). Coincident with the translation of the arc, the upper plate experienced shortening, the growth of doubly-vergent thrust belts, crustal thickening, and rock uplift (Duggen et al., 2003; Soto et al., 2008; Platt et al., 2013). In the Betics, contraction across the plate boundary was initially directed northward (Sanz De Galdeano, 1990; Lonergan, 1993; Platt et al., 2013). As the contraction continued into the foreland during the late Miocene, it slowed and progressively rotated to the northwest into its present orientation (Mazzoli and Helman, 1994; Rosenbaum et al., 2002). Active tectonics in the Betic Cordillera today is dominated by distributed NW-SE convergence of 4-6 mm/yr (Fernandez-Ibanez et al., 2007; Koulali et al., 2011; Gutshcer et al. 2012; Mancilla et al., 2013) and is

accommodated in part on NW-SE trending normal faults (Martínez- Martínez et al., 2006; Stich et al., 2006; Fernández-Ibáñez and Soto, 2008; Giaconia et al., 2014; 2015; Fig. 2).

The Sierra Nevada massif is a doubly-plunging, actively uplifting (Azañón et al., 2015) elongate dome, characterized by medium to low-grade metamorphic rocks stacked in north verging thrust sheets (Martinez-Martinez et al., 2002). Previous interpretations are that the Sierra Nevada dome was uplifted following top to the west extension and isostatic rebound after thrust belt formation (Martinez-Martinez et al., 2006). Alternatively, as many culminations exist in orogenic hinterlands, the massif could have been uplifted during contractional or transpressive strain (e.g., Bernini, 1990; Mitra et al., 1997).

To resolve whether the uplift of the Sierra Nevada dome was the result of extensional exhumation or a compressional orogenic culmination, we collected rock fabric (AMS) data in Plio-Pleistocene deposits around the massif to explore the presence of penetrative tectonic fabrics that can contribute additional constraints to the kinematics of dome emplacement. We focused sampling on unburied alluvial fan deposits in Neogene basins that surround the core of the structure (Fig. 3).

4.2 **Methods for Example I**

We collected samples from 6 sites distributed around Sierra Nevada, from all structural positions, around the massif in unburied Plio-Pleistocene fan deposits that range from poorly cemented to unconsolidated (Sanz de Galdeano and Vera, 1992; DR Table 1; Fig. 3). The ages of the deposits sampled were determined from published geologic maps (IGME-1:50,000 scale) and bridged the temporal gap between the late Miocene age metamorphic fabrics and the present day deformation field recorded by GPS geodesy and recent seismicity. At each site, three oriented samples were collected as independent blocks. Before removal from the outcrop, most blocks were hardened with a diluted (~50%) aqueous solution of sodium silicate (Fig. 4). In the laboratory, 2-3, oriented cubes ($8cm^3$) were cut from each block using non-magnetic Teflon knives and enclosed in standard cubic paleomagnetic boxes. The anisotropy of magnetic susceptibility (AMS) was determined with an Agico Kappabridge KLY-3S at Lehigh University. To determine magnetic mineralogy, a heating stage under the presence of an argon atmosphere and a cold stage accessory to the Kappabridge were used.

Commented [MOU1]: Could you provide some details about the fitting and how the proportions of paramagnetic to ferromagnetic estimates were determined, and for what temperature (e.g. the susceptibility response is 100% ferromagnetic at room temperature or across the whole spectrum?

Commented [MOU2]:

4.3 Results for Example I

Results from heating and cooling experiments show a complicated magnetic mineralogy composed of 100% ferromagnetic (magnetite or hematite) to 100% paramagnetic mineralogy (clays and iron-rich micas; Fig. 5). Since the kinematic interpretation of each of the specimen is the same regardless of magnetic mineralogy, the details of each specimen are not important for subsequent analysis. There is no correlation between the bulk magnetic susceptibility (k_m) and the anisotropy of the magnetic ellipsoid (P_j), so a comparison of the principal axis of susceptibility across the various structural positions around the Sierra Nevada massif specimens can provide useful kinematic information (Fig. 6a). Nearly all AMS ellipsoids are characterized by a low anisotropy degree (P_j) and oblate ellipsoid shape (T) (Jelinek, 1981; Fig. 6b). The AMS axes determinations record nearly the same axis orientations. At all sites around the Sierra Nevada, k_3 is nearly orthogonal to bedding. The principal elongation axes

means is preferentially oriented NNE-SSW to NE-SW (Fig. 3). The orientation of the site mean magnetic susceptibility axes, k_1, is horizontal or very shallowly plunging to the NE or SW (Fig 3). In general, k_1 and k_2 are in or near the bedding plane of the specimens and k_2 and k_3 do not form a girdle pattern in this principle plane.

Commented [MOU3]: Could you please describe the girdling of Kint and Kmin in site 45 and the oblique fabric of site 4? Is there any relation to the distinct Kmean of site 4 (which could be discussed in the next section)?

4.4 Discussion of Example I

The AMS principal axes show a consistency between sites (Fig. 3), so we combine the susceptibility axes orientation data in Figure 7. These combined data suggest that during deposition the phyllosilicate grains were oriented with their basal planes parallel or slightly imbricated to the depositional surface. Compaction during dewatering and lithification amplified the initial oblate depositional fabric and was coincident with the formation of the tectonic fabric. Regardless of the magnetic mineralogy of the specimens, a well-clustered minimum susceptibility axis (k_3) is present, which we interpret as a compaction fabric in these sedimentary deposits. The possibility of a primary depositional current fabric (imbrication) is unlikely because of an independent paleocurrent study on clast imbrication at Site 3 and Site 4, which shows an eastward rather than westward transport direction during deposition (Carrigan et al., 2018).

Irrespective of the structural position around the Sierra Nevada massif, all sites show a preferred orientation of k_1. The mean principal axis of maximum susceptibility is preferentially oriented at 030˚-210˚ (Figs.7 and 8). We interpret this as a tectonic fabric due to the tight clustering of k_1 and k_2, the relationship between k_1 and strike of dipping bedding at sites SN1, SN4, and SN6, and the lack of influence from sedimentary processes. In specimens dominated by phyllosilicate grains it is difficult to create a strong lineation by aligning grain crystallographic axes, however, an intersection lineation between slightly rotated clay grains orthogonal to a shortening direction has been observed (Henry, 1997; Parés et al., 2007; Martín-Hermández and Ferré, 2007; Borradaile and Jackson, 2010). The orientation of k_1 is consistent with the present day GPS velocity field, being oriented almost perfectly orthogonal to the direction of convergence of the Betic Cordillera to stable Africa (Nubia; Fig. 2; Gutscher et al., 2012), in good agreement with the mineral lineations recorded in the massif's core (Martinez-Martinez et al., 2002), and the Neogene brittle extensional structures and recent seismicity (Mancilla et al., 2013) in the orogen (Fig. 2). Because of the low strains and the orthogonal relationship between contractional and extensional principal directions it is not possible to distinguish the uplift processes of the Sierra Nevada massif with our results. The AMS ellipsoid orientations, mineralogic stretching lineation from the core of the Sierra Nevada massif, the nearby GPS velocity field, and recent fault slip, all have orientations consistent with the same strain field (Fig. 8). The principal elongation direction is interpreted to have persisted across different structural levels from Miocene time to the present (> 10 m.y.).

5 Example II: Northern Apennines, Italy

5.1. Geologic Setting of the Northern Apennines

The northern Apennines are an accretionary fold and thrust belt (Bally, et al., 1986) where crustal deformation, rock uplift, and topographic growth result from the ongoing subduction of Adria beneath Europe (Picotti and Pazzaglia, 2008; Carminati and Doglioni, 2012). The Apennine orogenic wedge initiated ~ 30 Ma along

188 the southern flank of the Alps (Le Pichon et al., 1971), and has grown at variable rates through the Neogene
189 dependent on the transfer of mass imbricated from the subducting plate (Picotti and Pazzaglia, 2008). Rapid
190 rollback of Adria with respect to Europe results in retreat and stretching of the upper plate, forming a wide zone of
191 back arc crustal extension. The Apennine wedge started to become emergent ~ 4 Ma (Picotti and Pazzaglia, 2008)
192 uplifting and exposing paired compressional and extensional deformation fronts near the trench and in the forearc
193 respectively, with the structural transition near the topographic culmination of the range (D'Agostino et al., 2001;
194 Carminati and Doglioni, 2012). Balanced cross-sections for the Apennines (Bally et al., 1986; Hill and Hayward,
195 1988) indicate ~130 to 150 km of subduction over the 30 m.y. history of the wedge, which indicates relatively slow
196 long-term rates at ~ 4 to 5 km/m.y. (4 – 5 mm/yr), similar to the GPS geodetic rates (Devoti et al., 2008; Caporali et
197 al., 2011; Bennett et al., 2012).
198 The northeastern Apennines, including the Umbria-Marche target region of this research, exposes
199 Mesozoic-early Cenozoic carbonates and middle-late Cenozoic mixed carbonate-siliciclastic rocks folded and
200 imbricated into northeast-vergent thrust sheets (Fig. 9). In Marche, these thrust sheets are located with carbonate
201 ridges and have inferred blind thrusts in their cores (Artoni, 2013). Further west in Umbria, the thrust sheets are
202 dissected by both east- and west-dipping high angle normal faults (Barchi et al., 1998; Fig. 9). Ongoing thrust
203 earthquakes beneath the Po Plain and Adriatic Sea (Pondrelli et al., 2006; Boccaletti et al., 2011) and normal-fault
204 sense earthquakes beneath the high Apennines (Lavecchia et al., 1994; Doglioni et al., 1999; Ghisetti and Vezzani,
205 2002; Chiaraluce et al., 2017) speak to concurrent shortening and extension in the wedge.
206 The paired deformation fronts in the northern Apennines Italy are convolved with an enigmatic, but active,
207 east-dipping (towards Adria), 14-15 km deep detachment called the Alto-Tiberina fault, that projects to the surface
208 west of the Apennine crest (Barchi et al., 1998; Pialli et al., 1998; Boncio et al., 2004; Chiaraluce et al., 2007; Eva et
209 al., 2014; Lavecchia et al., 2016; Fig. 9). This detachment is one of only a handful of low angle normal faults
210 globally that are demonstrably seismogenic (Hreinsdottir and Bennett, 2009; Valoroso et al., 2017), apparently in
211 contradiction to frictional fault reactivation theory that predicts that slip on low angle normal faults as extremely
212 unlikely (reviewed in Collettini, 2011). Most of the destructive seismicity in the high Apennines tends to nucleate
213 on west-dipping high angle normal faults that are antithetic to and sole into this east-dipping detachment (Galadini
214 and Galli, 2000; Boncio et al., 2004; Roberts and Michetti, 2004). The most destructive seismicity, including the
215 2016-17 earthquake sequence, is tightly focused along the highest crest of the Apennines where it is co-located with
216 young, underfilled, extensional basins, high angle normal faults that rupture the surface (Fig. 9), and geomorphic
217 evidence for an east-marching drainage divide. It is not known if the infrequent, but large historic earthquakes east
218 of the divide are indicative of new blind normal faults that have nucleated on the detachment, represent active
219 shortening, or alternatively are responding to a different stress field.
220 Imbricated foredeep and wedge-top basins contain a time-transgressive range of poorly consolidated
221 deposits that span the extensional and compressional regimes. Conceivably, shortening fabrics could be recorded in
222 lithofacies at the base of one of these basins when it was formed and filled in the shortening part of the wedge, only
223 to be superseded by stretching fabrics in overlying lithofacies as the basin was translated westward and into the
224 extending part of the wedge. Adriatic slope transverse rivers (Alvarez, 1999) traverse both the extending and

shortening parts of the wedge and contain Pleistocene alluvial deposits representing an AMS geodetic snapshot of the current crustal strains. Published AMS data from the thrust belt shows strike-parallel (NE-SW and horizontal) extension that is perpendicular to compression and shortening directions (Caricchi et al., 2016). To confirm these data towards the southeast and to better locate the kinematic transition region between the contracting and extending regions of the overlying Eurasian plate, we sampled AMS data in Oligocene and younger units, including Quaternary deposits in a NE-SW oriented corridor across the thrust belt (Fig. 9).

5.2 Methods for Example II

Sampling in the Apennines was designed to identify the location of the modern extensional front. Field collection and specimen preparation occurred as in Example I from Spain, with unconsolidated samples being hardened with sodium silicate before or just after orienting and removal from the outcrop (Fig. 4). We collected samples from 17 sites from sedimentary rocks and poorly consolidated sediments from Late Eocene to late Pleistocene age, with a focus on late Miocene-Pliocene argillaceous marine deposits (Table A1). The Italian specimens were prepared and rock magnetic data was acquired in the Archeomagnetism Laboratory at CENIEH (Spain). The AMS of the collected specimens was measured on a MFK1-FA Kappabridge (AGICO Instruments), a fully automated inductive bridge, at a frequency of 976 Hz and a field of 200 A/m. Analysis software (Saphyr6, by AGICO) creates a complete susceptibility tensor. Rock magnetic measurements included isothermal remanent magnetization (IRM) acquisition experiments up to 1T and hysteresis curves to determine the relative contribution of ferromagnetism and paramagnetism to the total susceptibility tensor. These experiments were carried out with a Vibrating Sample Magnetometer (VSM; Micromag 3900).

5.3 Results of Example II

Samples from the Apennines have variable magnetic mineralogy and include a wider range of lithologies and ages than the Betics sampling. Samples from sites AP2 and AP7 (Bisciaro Fm.) are dominated by diamagnetic calcite and negative mean susceptibility, which precludes any meaningful analysis of the AMS axes orientations. At most other sites, axes orientations were interpretable and the k_1 orientation is shown in Figure 10 for spatial comparison. At 1T field, the magnetization was not fully-saturated, indicating the presence of hematite in addition to lower coercivity magnetite as the dominant ferromagnetic components (Heller, 1978). Still, the bulk magnetic susceptibility is dominated by paramagnetism as revealed by the hysteresis curves (Fig. 11). The contribution of paramagnetic grains suggests that the measured magnetic fabric can be used as a proxy for phyllosilicate grains preferred orientation, therefore, the AMS principal axes are indicators of the orientation of the strain axes orientation (e.g., Soto et al., 2009).

Representative examples of AMS fabrics are shown in Figure 12. The mean susceptibility shows no positive correlation with the shape parameter or anisotropy degree (T, P_j; Figure 13). Similar to the data from Spain, the AMS ellipsoids from the Italian specimens indicate low P_j values, revealing a low degree of grain shape preferred orientation and low strains. The AMS axes distribution are particularly clear in specimens of the argillaceous and semi-consolidated Pliocene Argille Azzurre Fm. At all sites, k_1 axes orientations are shown as a function of rock

formation, as well as the sites in which k_3 is perpendicular to bedding (Fig. 10). All interpretable specimens from the Apennine Range samples, including the Pleistocene fluvial deposits, generate a site mean AMS fabric consistent with contraction and shortening in the wedge.

5.4 Discussion for Example II

Irrespective of sample age, we interpret AMS ellipsoids that have the magnetic lineation in a NW-SE orientation as recording contraction as this is the main trend of the fault traces and strike of bedding and topography (Fig. 10). The k_1 axis orientation is orthogonal to the rock transport and crustal shortening directions as recorded in GPS geodesy data and seismology (Fig. 9). A few sites do not provide interpretable kinematic results because the axes directions are scattered and suggest inconsistent strain directions. The calcareous marls of the Bisciaro Fm. (AP2, AP7) have a poorly formed AMS fabric. In these specimens, the mean susceptibility is negative and dominated by diamagnetism, most likely calcite. The absence of a compactional fabric in carbonate dominated specimens (AP2, AP7) likely indicates that these sediments lithified by cementation soon after deposition.

In general, the distribution of the principal axes of the AMS ellipsoid does not significantly vary with stratigraphic age or structural position. For example, the oldest specimens collected from Eocene-middle Miocene marls and Pliocene siliciclastics rocks (AP6, AP14, AP17), uniformly show AMS fabrics consistent with contractional deformation of the orogenic wedge (Fig. 10). Most importantly, sites collected from thrust structures that are currently in an extending regime (AP11, AP12, AP13) implies that either the AMS fabrics was locked after the original deformation due to the high strain required to rotate grain pairs, or that subsequent extension has not affected the previous AMS fabric. (e.g., Larrasoña et al., 2004). The same is true for middle and late Miocene siliciclastic deposits astride the Marche ridge (AP3, AP9) where the current orientations of crustal stresses from fault and earthquake data are ambiguous. Pliocene and Pleistocene samples from near the toe of the orogenic wedge show an orientation consistent with ongoing shortening (AP4, AP5, AP8). Wegmann and Pazzaglia (2009) also report ongoing shortening in this region as evidenced by fluvial terrace folding above the Filottrano thrust, which we cross at the location of AP4.

The kinematic transition zone in central Italy aligns with the topography, the seismicity (Pondrelli et al., 2006) and the GPS geodesy (Bennett et al., 2012; Fig. 9). Our AMS data does not improve on the location of the transition zone because of the lack of samples from Plio-Pleistocene deposits directly northeast of the drainage divide (Fig. 10). Unfortunately, the one Pleistocene river terrace deposit northeast of the divide (AP10) has indeterminate axes. As such, our AMS results are not able to support the idea that there is an apparent rotation of the principal compressive stress between the Adriatic coast and the Marche ridge associated with wedge-scale pore-pressure variations (Peacock et al., 2017). Furthermore, the AMS is unable to determine the stress field responsible for the large historic earthquakes in the region between the drainage divide and the Marche Ridge. If earthquakes in the region are related to blind normal faults with tips breaking up-section from the Alto-Tiburina detachment (Fig. 9), a possible rationale is that according to extensional critical wedge theory (Davis et al., 1983), a wedge with a taper greater than some critical value is unable to slide over its basal detachment until sufficient wedge thinning on connecting faults reduces the surface slope and wedge taper below the critical value (Xiao et al., 1991). Suitable

Commented [MOU4]: What are these fabrics like, other than poorly formed: are they scattered and inconsistent, inverted... again, it may useful to take a look at the absolute eigenvalues of the fabrics and determine which are really the largest and smallest, although, of course they will represent the summation of all mineralogical contributions, adding to the complication.

deposits do outcrop in this critical region, so additional field work and AMS analyses may yet bear light on this problem.

6 Conclusions

The AMS technique provides an effective way to identify both modern and paleo-kinematics from sediments and sedimentary rocks largely independent of the magnetic mineralogy of a specimen. Stratigraphically controlled AMS measurements are a deep-time, paleogeodetic technique that can be combined with structural geology, GPS geodesy, and seismic data to collectively describe the kinematics of active orogens and to better understand the nature of seismic hazards. In both the Betic Cordillera (Example I) and northern Apennines (Example II), weak but well-organized penetrative AMS fabrics were recovered from young unconsolidated and unburied rocks that could not be analyzed with more traditional methods. In the Betic Cordillera we established a long-term consistency to the strain field from the Late Miocene to the present from unburied, young deposits around Sierra Nevada. For the northern Apennines all studied sites, regardless of site's stratigraphic age, ubiquitously record NW-SE oriented k_1 axes orientations, irrespective of structural position. Contractional strains in the most southwest-located samples are likely locked into the rocks and do not record superposed penetrative extension. In any case, the recovered magnetic fabric orientation successfully determined the kinematics of an area near the synorogenic surface, in the still contracting orogen toe region.

Author Contribution

Anastasio, Parés, and Berti conceived the Spanish project and completed sampling, sample preparation, measurement, and analyses. Anastasio and Pazzaglia conceived the Italian project. Anastasio, Pazzaglia, Montanari, and Karnes completed the Italian sampling. Anastasio and Parés prepared the Italian specimens, measured the samples, and analyzed the results. Anastasio, Pazzaglia, Fisher, Berti, and Kodama analyzed results and drafted figures for the manuscript. Anastasio and Pazzaglia wrote the first draft of the manuscript and edited each subsequent draft. Parés, Kodama, Berti, and Montanari edited multiple drafts of the manuscript. Anastasio completed the final edits.

Competing Interests

The authors all declare that they have no conflict of interest.

Special Issue Statement

This paper is intended for the special issue on "Tools, data and models for 3D seismotectonics: Italy a key natural laboratory" Rita De Nardis, Massimiliano Porreca, Ramon Arrowsmith, Luca De Siena, Beatrice Magnani, Frank Pazzaglia, and Federico Rossetti, editors.

7 Acknowledgements

The authors thank Andrea Rodriguez Rubio, Alondra Jimenez Perez, Isabel Hernando Alonso of CENIEH for laboratory assistance and the Association “Le Montagne di San Francesco” for logistical support during the sampling campaign in the Umbria-Marche Apennines. Agico is acknowledged for Anisoft software and Lisa Tauxe is thanked for PmagPy software (Tauxe et al., 2016) used to analyze the AMS data presented here. Anastasio thanks CENIEH and Parés for hosting his academic leave during the fall 2019 semester. We thank Drs. Dario Biardello and Ruth Soto for their reviews of the manuscript.

8 References

Alvarez, W. Drainage on evolving fold-trust belts: a study of transverse canyons in the Apennines. Basin Res, 11, 267-284. 1999.

Artoni, A.: The Pliocene-Pleistocne stratigraphic and tectonic evolution of the central sector of the Western Periadriatic Basin of Italy. Mar and Petrol Geol, 42, 82-106. 2013.

Averbuch, O., Delamotte, D. F., and Kissel, C.: Magnetic fabric as a structural indicator of the deformation path within a fold thrust structure – a test case from the Corbieres (NE Pyrenees, France). J Struct Geol, 14, 461-474. 1992.

Azañón, J. M, Galve, J. P., Perez-Pena, J. V., Giaconia, F., Carvajal, R., Booth-Rea, G., Jabaloy, A., Vazquez, M., Azor, A., and Roldan, F. J.: Relief and drainage evolution during the exhumation of the Sierra Nevada (SE Spain): Is denudation keeping pace with uplift? Tectonophysics, doi:10.1016/j.tecto.2015.06.015. 2015.

Balley, A. W., Burbi, L., Cooper, C., and Ghelardoni, R.: Balanced sections and seismic reflection profiles across the central Apennines. Mem Soc Geol Ital, 35, 257-310. 1986.

Barchi, M., De Feyter, A., Magnani, M., Minelli, G., Pialli, G. and Sotera, B.: Extensional tectonics in the Northern Apennines (Italy): evidence from the CROP03 deep seismic reflection line. Mem Soc Geol Ital, 52, 528–538. 1998.

Bartole, R. The north Tyrrhenian-northern Apennines post-collisional system: Constraints for a geodynamic model. Terra Nova, 7, 7 – 30. 1995.

Basili, R. and Barba, S. Migration and shortening rates in the northern Apennines, Italy: Implications for seismic hazard. Terra Nova, 19, 462 – 468. 2007.

Beccaluva, L., G. Gabbianelli, F. Lucchini, P.L. Rossi, and Savelli. C: Petrology and K/Ar Ages of volcanics dredged from the Eolian seamounts: Implications for geodynamic evolution of the Southern Tyrrhenian Basin. Earth Planet Sc Lett 74, 187– 208. doi:10.1016/0012-821X(85)90021-4. 1985.

Bennett, R. A., Serpelloni, E., Hreinsdottir, S., Brandon, M. T., Buble, G., Basic, T., Casale, G., Cavaliere, A., Anzidei, M., Marjonovic, M., Minelli, G., Molli, G., and Montanari, A.: Syn-convergent extension observed using the RETREAT GPS network, northern Apennines, Italy. J Geophys Res, 117, B04408, doi:10.1029/2011JB008744. 2012.

Bernini, B.M. The role of transpression movements in the evolution of Neogene basins of the Betic Cordillera. An Tect, 4 ISSN: 0394-5596. 1990.

Bice, D., Lacroce, M., McGee, D., and Montanari, A.: Late Pleistocene tectonic tilting of the Frasassi anticline from offset stalagmites in the Grotta Grande del Vento (Marche, Italy), in Koeberl, C., and Bice, D.M., eds., 250 Million Years of Earth History in Central Italy: Celebrating 25 Years of the Geological Observatory of Coldigioco. Geo S Am S 542, 447–457. https://doi.org/10.1130/2019.2542(25). 2019.cb

Biedermann, A.,R.,: Magnetic Anisotropy in Single Crystals: A Review. Geoscien, v. 8, 302. 10.3390/geosciences8080302 2018.

Boccaletti, M., Corti, G., and Martelli, L. Recent and active tectonics of the external zone of the Northern Apennines (Italy). Int J of Earth Sci, (Geol Rundsch), 100, 1331-1348, DOI: 10.1007/s00531-010-0545-y. 2011.

Boncio, P., and Lavecchia, G. Pace, B. Defining a model of 3D seismogenic sources for Seismic Hazard Assessment applications: the case of central Apennines (Italy). J Seismol, 8, 407–425. 2004.

Borradaile, G., J., Werner, T.: Magnetic anisotropy of some phyllosilicates. Tectonophysics v. 225, 223-248. 1994

Borradaile, G. J., and Jackson, M.: Anisotropy of magnetic susceptibuility (AMS): magnetic petrofabrics of deformed rocks, in Martîn-Hernåndez, F. Lüneburg, C.M. Aubourg, and M. Jackson (eds.). Magnetic Fabric: Methods and Applications. Geo Soc Spec Publ, 238, 299-360. London, 0305-8719/04/. 2004.

Borradaile, G. J., and Jackson, M.: Structural geology, petrofabrics and magnetic fabrics (AMS, AARM, AIRM). J Struct Geol, 32, 1519–1551. doi: 10.1016/j.jsg.2009.09.006. 2010.

Borradaile, G. J., and Henry, B.: Tectonic applications of magnetic susceptibility and its anisotropy. Earth Sci Rev, 4, 49-93. 1997.

406
407 Borradaile, G. J., and Tarling, D. H.: The influence of deformation mechanisms on magnetic fabrics in weakly
408 deformed rocks. Tectonophysics, 77, 151-168. 1981.
409
410 Borradaile, G.J., Lagroix, F.: The enhancement of magnetic fabrics un high grade gneiss. Geophysical Research
411 Letters. v. 27, 2413-2416.. https://doi.org/10.1029/2000GL008522. 2000.
412
413
414 Burmeister, K. C., Harrison, M. J., Marshak, S., Ferre, E, C., and Bannister, R. A.: 2009. Comparison of Fry strain
415 ellipse and AMS ellipsoid trends to tectonic fabric trends in very low-strain sandstone of the Appalachian fold-thrust
416 belt. J Struct Geol, 9, 1028-1038. 2009.
417
418 Butler, R. F.: Paleomagnetism: magnetic domains to geologic terranes. Blackwell Scientific Publications, Boston.
419 1992.
420
421 Caporali, A., Barba, S., Carafa, M.M.C., Devoti, R., Pietrantonio, G., and Riguzzi, F.: Static stress drop as
422 determined from geodetic strain rates and statistical seismicity. J Geophys Res, 116, B02410.
423 doi:10.1029/2010JB007671. 2011.
424
425 Caricchi, C., Cifelli, F., Kissel, C., Sagnotti, L., and Mattei, M.: Distinct magnetic fabric in weakly deformed
426 sediments from extensional basins and fold-and-thrust structures in the Northern Apennine orogenic belt (Italy):
427 Tectonics, 35, 238-256, doi:10.1002/2015TC003940. 2016.
428
429 Carminati, E., and Doglioni, C.: Alps vs. Apennines: The paradigm of a tectonically asymmetric Earth. Earth Sci
430 Rev, 112, 67-96. 2012.
431
432 Carrigan, J. H., Anastasio, D. J., Berti, C., and Pazzaglia, F. J.: Post-Messinian Drainage
433 Reorganization in an Active Orogen, Betic Cordillera, Spain. Geo Soc Am Abstracts with Programs. 2018.
434
435 Cavinato, G.P. and DeCelles, P.: Extensional basins in the tectonically bimodal central Apennines fold-thrust belt,
436 Italy. Response to corner flow above a subducting slab in retrograde motion. Geology, 27, 955–958. 1999.
437
438 Chiaraluce, L., Chiarabba, C., Collettini, C., Piccinini, D., and Cocco, M.: Architecture and mechanics of an active
439 low-angle normal fault: Alto Tiberina Fault, northern Apennines, Italy. J Geophys Res, 112, B10310,
440 doi:10.1029/2007JB005015. 1999.
441

Chiaraluce, L. Barchi, M. R., Carannante, S., Collettini, C., Mirabella, F., Pauselli, C., and Valoroso, L. The role of rheology, crustal structures and lithology in the seismicity distribution of the northern Apennines. Tectonophysics, 694, 2810-291. 2017.

Cloos, E.: Oolite Deformation in South Mountain Fold, Maryland. Geo Soc Am Bull, 58, 843-918. 1947.

Collettini, C.: The mechanical paradox of low-angle normal faults: Current understanding and open questions. Tectonophysics, 510, 253-268. 2011.

D'Agostino, N., Jackson, J. A., Dramis, F., and Funiciello, R.: Interactions between mantle upwelling, drainage evolution and active normal faulting: an example from the central Apennines (Italy). Geophys J Int, 147, 475-497. 2001.

Davis, D., Suppe, J., and Dahlen, F. A.: Mechanics of fold-and-thrust belts and accretionary wedges. J Geophys Res, 88 (B2),1153-1172. 1983.

Devoti, R., Riguzzi, F., Cuffaro, M., and Doglioni, C.: New GPS constraints on the kinematics of the Apennines subduction. Earth and Planet Sci Lett, 273, 163–174. 2008.

Doglioni, C., Harabaglia, P., Merlini, S., Mongelli, F., Peccerillo, A.T., and Piromallo, C. 1999. Orogens and slabs vs. their direction of subduction. Earth Sci Rev, 45, 167–208. 1999.

Duggen S., Hoernle, K., van den Bogaard, P., Rüpke, L., & Morgan, J.P.: Deep roots of the Messinian Salinity Crisis. Nature, 422, 602-606. DOI: 10.1038/nature01553. 2003.

Elter, P., Giglia, G., Tongiorgi, M., and Trevisan, L.: Tensional and compressional area in the recent (Tortonian to present) evolution of the Northern Apennines. B Geofis Teor Appl, 17, 3-18. 1975.

Eva, E., Solarino, S., and Boncio, P.: HypoDD relocated seismicity in northern Apennines (Italy) preceding the 2013 seismic unrest: seismotectonic implications for the Lunigiana-Garfagnana area. B Geofis Teor Appl, 55, 739–754. 2014.

Fernández-Ibáñez, F., and Soto., J.I.: Crustal Rheology and Seismicity in the Gibraltar Arc (western Mediterranean). Tectonics, 27. doi:10.1029/2007TC002192. 2008.

Fernandez-Ibañez, F., Soto, J. I., Zoback, M. D., and Morales, J.: Present-day stress field in the Gibraltar Arc (western Mediterranean). J Geophy Res: Solid Earth, 112 (B08404) doi:10.1029/2006JB004683. 2007.

Galadini, F. and Galli, P.: Active tectonics in the central Apennines (Italy) - input data for seismic hazard assessment. Nat Hazards, 22, 225–270. 2000.

Ghisetti, F., and Vezzani, L.: Normal faulting, transcrustal permeability and seismogenesis in the Apennines (Italy). Tectonophysics, 348, 155–168. 2002.

Giaconia, F., Booth-Rea, G., Martínez-Martínez, J. M., Azañón, J. M., Storti, F., and Artoni, A.: Heterogeneous Extension and the Role of Transfer Faults in the Development of the Southeastern Betic Basins (SE Spain). Tectonics, 33, 2467–89. doi:10.1002/2014TC003681. 2014.

Giaconia, F., Booth-Rea, G., Ranero, C.R., Gràcia, E., Bartolome, R., Calahorrano, A., Lo Iacono, C., Vendrell, M.G., and Cameselle, A.L.: Compressional tectonic inversion of the Algero-Balearic basin: Latemost Miocene to present oblique convergence at the Palomares margin (Western Mediterranean). Tectonics, 34, 1516-1543. https://doi.org/10.1002/2015TC003861. 2015.

Gutscher, M.A., Dominguez, S., Westbrook, G.K., Le Roy, P., Rosas, F., Duarte, J. C., Terrinha, P., Miranda, J.M., Graindorge, D., Gailler, A., Sallares, V., and Bartolome, R.: The Gibraltar Subduction: A Decade of New Geophysical Data. Tectonophysics, 574-575, 72–91. doi:10.1016/j.tecto.2012.08.038. 2012.

Heller, F.: Rockmagnetic studies of Upper Jurassic limestones from southern Germany. J Geophys, 44, 525-543. 1978.

Henry B.: The magnetic zone axis: a new element of magnetic fabric for the interpretation of magnetic lineation. Tectonophysics, 271, 325—331. 1997.

Hill, K. and Hayward, A.: Structural constraints on the Tertiary plate tectonic evolution of Italy. Mar Petrol Geol, 5, 2 – 16. 1988.

Housen, B., A., Richter, C., and van der, Pluijm, B., A.: Composite magnetic anisotropy fabrics: experiments, numerical models, and implications for the quantification of rock fabrics. Tectonophysics, V. 220, 1-12. 1993.

Hreinsdóttir, S., and Bennett, R.A.: Active aseismic creep on the Alto Tiberina low-angle normal fault, Italy. Geology 37, 683–686. https://doi.org/10.1130/G30194A.1. 2009

516 Hrouda, F.: Magnetic Anisotropy of Rocks and Its Application in Geology and Geophysics.
517 Geophysical Surveys, 5, 37-82. http://dx.doi.org/10.1007/BF01450244. 1982.
518
519 Jelinek, V.: Characterization of the magnetic fabric of rocks. Tectonophysics, 79, 63-67. 1981.
520
521 Kligfield, R., Owens, W. H., and Lowrie, W.: Magnetic susceptibility anisotropy, strain and progressive deformation
522 in Permian sediments from the Maritime Alps (France). Earth Planet Sc Lett, 55, 181–189. doi: 10.1016/0012-
523 821X(81)90097-2. 1981.
524
525 Kodama, K. P. and Sun, W-W.: Magnetic anisotropy as a correction for compaction-caused
526 paleomagnetic inclination shallowing. Geophys J Int, 111, 465-469. 1992.
527
528 Koulali, A., Ouazar, D., Tahayt, A. King, R. W., Vernant, P., Reilinger, R. E., McClusky, S.,
529 Mourabit, T., Davila, J. M., and Amraoui, N.: New GPS constraints on active deformation along the Africa-Iberia
530 plate boundary: Earth Planet Sc Lett, 308, 211-217. 2011.
531
532 Larrasoaña, J.C., Pueyo, E.L., and Parés, J.M.: An integrated AMS, structural, paleo- and rock-magnetic study of the
533 Eocene marine marls from the Jaca-Pamplona basin (Pyrenees, N Spain); new insights into the timing of magnetic
534 fabric acquisition in weakly deformed mudrocks. Magnetic Fabric: Methods and Applications (Martín-Hernández,
535 F., Lüneburg, C.M., Aubourg, C. y Jackson, M. Eds.). Geol Soc Sp Publ, London, 238, 127-143. 2004.
536
537 Latta, D.K. and Anastasio, D.J.: Multiple scales of mechanical stratification and décollement fold kinematics, Sierra
538 Madre Oriental foreland, northeast Mexico. Jof Struct Geol, 29, 1241-1255. 2007.
539
540 Lavecchia, G., Adinolfi, G. M., Nardis, R., Ferrarini, F., Cirillo, D., Brozzetti, F., De Matteis, R., Festa, G., and
541 Zollo, A.: Multidisciplinary inferences on a newly recognized active east dipping extensional system in Central
542 Italy. Terra Nova, 29, 77-89. 2016.
543
544 Lavecchia, G., Brozzetti, F., Barchi, M., Menichetti, M., and Keller, J.V.:. Seismotectonic zoning in east-central
545 Italy deduced from an analysis of the Neogene to present deformations and related stress fields. Geol Soc Am Bull,
546 106, 1107–1120. 1994.
547
548 Le Pichon, X., G. Pautot, J. M. Auzende, and Olivet, J. L.: La Mediterranee occidentale depuis l'oligocene; scheme
549 d'evolution: The western Mediterranean since the Oligocene; evolutionary scheme, Earth Planet Sc Lett, 13, 145 –
550 152. 1971.
551
552 Le Pichon, X, and Angelier, J.: The Hellenic arc and trench system: a key to the neotectonic

553 evolution of the eastern Mediterranean area. Tectonophysics, 60, 1-42. 1979.
554
555 Lonergan, L.: Timing and kinematics of deformation in the Malaguide Complex, internal zone of the Betic
556 Cordillera, southeast Spain. Tectonics, 12, 460-476 https://doi.org/10.1029/92TC02507. 1993.
557
558 Lonergan, L., and White, N.: Origin of the Betic-Rif Mountain Belt. Tectonics, 16, 504–22.
559 doi:10.1029/96TC03937. 1997.
560
561 Makris, J., Egloff, F., Nicolich, R., and Rihm, R.: Crustal structure from the Ligurian Sea to the Northern
562 Apennines-a wide angle seismic transect. Tectonophysics, 301, 305 – 319. 1999.
563
564 Mancilla, FdL., Stich, D., Berrocoso, M., Martin, R., Morales, J., Fernandez-Ros, A., Paez, R.,
565 and Perez-Pena, A.: Delamination in the Betic Range: Deep structure, seismicity, and GPS motion. Geology, 41,
566 307-310. 2013.
567
568 Martin-Hernandez, F. and Hirt, A.M.: The anisotropy of magnetic susceptibility in biotite,
569 muscovite and chlorite single crystals. Tectonophysics, 367, 13-28. 2003.
570
571 Martín-Hernández, F. and Ferré, E.C.: Separation of paramagnetic and ferrimagnetic anisotropies. A review. J
572 Geophys Res: Sol Ea 112 (B3), https://doi.org/10.1029/2006JB004340. 2007.
573
574 Martínez-Martínez, J. M., Booth-Rea, G., Azañón, J. M., and Torcal, F.: Active transfer fault
575 zone linking a segmented extensional system (Betics, Southern Spain): Insight into heterogeneous extension Driven
576 by Edge Delamination. Tectonophysics, 422, 159–73. doi:10.1016/j.tecto.2006.06.001. 2006.
577
578 Martınez-Martınez, J. M., Soto, J. I. and Balanyá, J.C.: Orthogonal folding of extensional detachments: Structure
579 and origin of the Sierra Nevada elongated dome (Betics, SE Spain). Tectonics, 21, doi:10.1029/2001TC001283.
580 2002.
581
582 Mattei, M., Sagnotti, L., Faccenna, C., and Funiciello, R.: Magnetic fabric of weakly deformed clay-rich sediments
583 in the Italian peninsula: Relationship with compressional and extensional tectonics. Tectonophysics, 271, 107-122.
584 1997.
585
586 Mattei, M., D'Agostino, N., Zananiri, I., Kondopoulou, D., Pavlides, S., Spatharas, V.: Tectonic evolution of fault-
587 bounded continental blocks: Comparison of paleomagnetic and GPS data in the Corinth and Megara basins
588 (Greece). Solid Earth,v. 109, B02106, doi:10.1029/2003JB002506. 2004
589

590 Mazzoli, S. and Helman, M.: Neogene patterns of relative plate motion for Africa-Europe:
591 some implications for recent central Mediterranean tectonics. Geol Rund, 83, 464–68. 1994.
592
593 Milia, A., Turco, E., Pierantoni, P. P., and Schettino, A.: Four-dimensional tectono- stratigraphic evolution of the
594 southeastern Peri-Tyrrhenian Basins (Margin of Calabria, Italy). Tectonophysics, 476, 41–56,
595 doi:http://dx.doi.org/10.1016/j.tecto.2009.02.030. 2009.
596
597 Mitra, G., and Sussman, A.J.: Structural evolution of connecting splay duplexes and their
598 implications for critical taper; an example based on geometry and kinematics of the Canyon Range culmination,
599 Sevier Belt, central Utah. J Struct Geol, 19, 503-521. 1997.
600
601 Papazachos, B. C., Karakostas, V. G., Papazachos, C. B., and Scordilis, E. M.: The geometry of the Wadati-Benioff
602 zone and lithospheric kinematics in the Hellenic arc. Tectonophysics, 319, 275-300. 2000.
603
604 Parés, J. M., Hassold, N. J. C., Rea, D. K., and van der Pluijm, B. A.: Paleocurrent directions from paleomagnetic
605 reorientation of magnetic fabrics in deep-sea sediments at the Antarctic Peninsula Pacific margin (ODP Sites 1095,
606 1101). Mar Geol, 242, 4, 261-269. 2007.
607
608 Parés, J. M. and van der Pluijm, B. A.: Evaluating magnetic lineations (AMS) in deformed rocks. Tectonophysics,
609 350, 283-298. 2002.
610
611 Parés, J.M.:. How deformed are weakly deformed mudrocks? Insights from magnetic anisotropy. Geol Soc Sp, 238,
612 191-203. 2004.
613
614 Parés, J.M. and van der Pluijm, B.: Phyllosilicate fabric characterization by low temperature
615 anisotropy of magnetic susceptibility (LT-AMS). Geophys Res Lett, 29, 68-1-68-4. 2003.
616
617 Peacock, C. P., Tavernelli, E., and Anderson, M. W.: Interplay between stress permutations and overpressure to
618 cause strike-slip faulting during tectonic inversion. Terra Nova, 29, 61-70, doi:10.1111/ter.12249. 2017.
619
620 Peters, C. and Dekkers, M. J.: Selected room temperature magnetic parameters as a function of mineralogy,
621 concentration and grain size. Phys Chem Earth, 28, 659-667. 2003.
622
623 Pialli, G., Barchi, M., and Minelli, G., (eds.): Results of the CROP 03 deep seismic reflection profile. Mem Soc
624 Geol Ital, 52, 647 pp. 1998.
625

626 Picotti, V. and Pazzaglia, F. J.: A new active tectonic model for the construction of the Northern Apennines
627 mountain front near Bologna (Italy). J Geophys Res, 113, B08412, doi: 10.1029/2007JB005307. 2008.
628
629 Platt J. P., Anczkiewicz R., Soto J. I., and Kelley S. P., Thirlwall, M.: Early Miocene continental subduction and
630 rapid exhumation in the western Mediterranean. Geology, 34, 981-984. 2006.
631
632 Platt, J. P., Behr, W. M., Johanesen, K., and Williams, J.R.: The Betic-Rif Arc and its orogenic hinterland: a review.
633 Annu Rev Earth and Pl Sc, 41, 313–357. doi:10.1146/annurev-earth-050212-123951. 2013.
634
635 Pondrelli, S., Salimbeni, S., Ekstrom, G., Morelli, A., Gasperini, P. and Vannucci, G.: The Italian CMT dataset
636 from 1977 to the present. Phys Earth Planet Int, 159, 286–303, doi:10.1016/j.pepi.2006.07.008. 2006.
637
638 Porreca, M. and Mattei, M.: AMS fabric and tectonic evolution of Quaternary intramontane extensional basins in the
639 Picentini Mountains (southern Apennines, Italy): Int J Earth Sci, 101, 863-877. 2012.
640
641 Ramsay, J. G. and Huber, M. I.: The Techniques of Modern Structural Geology, Vol. 1. Academic Press, San
642 Diego. 1984.
643
644 Richter, C., van der Pluijm, B., and Housen, B.: The quantification of crystallographic preferred orientation using
645 magnetic anisotropy. J Struct Geol, 15, 113–116. 1993.
646
647 Roberts, G.P. and Michetti, A.M.: Spatial and temporal variations in growth rates along active normal fault systems:
648 an example from the Lazio-Abruzzo Apennines, central Italy. J Struct Geol, 26, 339–376. 2004.
649
650 Rosenbaum, G., Lister, G. S., and Duboz, C.: Reconstruction of the Tectonic Evolution of the Western
651 Mediterranean since the Oligocene. Tectonophysics, 359, 117-129. 2002.
652
653 Rovida, A., Locati, M., and Camassi, R.: The Italian earthquake catalogue CPTI15. B Earthq Eng, 18, 2953–2984.
654 2020.
655
656 Sagnotti, L., Speranza, F., Winkler, A., Mattei., and Funiciello, R.: Magnetic fabric of clay sediments from the
657 external northern Apennines (Italy). Phys Earth Planet Int, 105, 73-93. 1998.
658
659 Sanz De Galdeano, C.: Geologic evolution of the Betic Cordilleras in the Western Mediterranean, Miocene to the
660 present. Tectonophysics, 172, 107-119. https://doi.org/10.1016/0040-1951(90)90062-D. 1990.
661

662 Sanz De Galdeano, C. and Vera, J. A.: Stratigraphic record and palaeogeographical context of the Neogene basins in
663 the Betic Cordillera, Spain. Basin Res, 4, 21–36. 1992.
664
665 Schwehr, K., Tauxe, L., Driscoll, N., and Lee, H.: Detecting compaction disequilibrium with anisotropy of magnetic
666 susceptibility. Geochem, Geophy, Geosy, 7, Q11002. doi: 10.1029/2006GC001378. 2006.
667
668 Soto, J.I., Fernandez-Ibanez, F., Fernandez, M., and Garcia-Casco, A.: Thermal structure of the crust in the
669 Gilbralter Arc: Influence on active tectonicsin the western Mediterranean. Geochem, GeophyGeosy, 9,
670 http://dx.doi.org/10.1029/2008GC002061. 2008.
671
672 Soto, R., Larrasoaña, J.C., Arlegui, L.E., Beamud, E., Oliva-Urcia, B., and Simón, J.L.: Reliability of magnetic
673 fabrics of weakly deformed mudrocks as a palaeostress indicator in compressive settings. J Struct Geol, 31, 512 -
674 522. 2009.
675
676 Stich, D., Serpelloni, E., Mancilla, F. d. L., and Morales, J.: Kinematics of the Iberia– Maghreb plate contact from
677 seismic moment tensors and GPS observations. Tectonophysics, 426, 295–317, doi:10.1016/j.tecto.2006.08.004.
678 2006.
679
680 Tarling, D.H. and Hrouda, F.: The Magnetic Anisotropy of Rocks. Chapman and Hall, London, UK. 1993.
681
682 Tauxe, L.: Paleomagnetic Principles and Practices. Kluwer Academic Publishers. Norwell,
683 MA. 2002.
684
685 Tauxe, L., Shaar, R. Jonestrask, L., Swanson-Hysell, N.,L., Minnett, R., Koppers, A.,A.,P., Constable, C.,G., Jarboe,
686 N., Gaastra, K., and Fairchild, L.: PmagPy: Software package for paleomagnetic data analysis and a bridge to the
687 Magnetics Information Consortium (MagIC) Database. Geochemistry, Geophysics, Geosystems. v. 17, 2450-2463.
688 doi.org/10.1002/2016GC006307. 2016.
689
690 Tarquini S., Vinci S., Favalli M., Doumaz F., Fornaciai A., Nannipieri L.: Release of a 10-m-resolution DEM for
691 the Italian territory: Comparison with global-coverage DEMs and anaglyph-mode exploration via the web,
692 Computers & Geosciences , 38, 168-170. doi: doi:10.1016/j.cageo.2011.04.018. 2012.
693
694 Wegmann, K. W. and Pazzaglia, F. J.: Late Quaternary fluvial terraces of the Romagna and
695 Marche Apennines, Italy: Climatic, lithologic, and tectonic controls on terrace genesis in an active orogen.
696 Quaternary Sci Rev, 28, 137-165. 2009.
697

Weill, A.,B., and Yonkee, A.: Anisotropy of magnetic susceptibility in weakly deformed red beds from the Wyoming salient, Sevier thrust belt: Relations to layer-parallel shortening and orogenic curvature. Lithosphere. v. 1, 235-256. doi.org/10.1130/L42.1. 2009.

Valoroso, L., Chiaraluce, L., Di Stefano, R., and Monachesi, G.: Mixed-mode slip behavior of the Alto Tiberina low-angle normal fault system (Northern Apennines, Italy) through high-resolution earthquake locations and repeating events. J Geophys Res: Sol Ea, 122, 10,220-10,240. 2017.

Xiao, H-B., Dahlen, F. A., and Suppe, J.: Mechanics of extensional wedges. J Geophys Res, 96, 10,301-10,318. 1991.

Figure Captions

Figure 1. Topography and bathymetry of the western Mediterranean showing (a) the Betic orogen, southern Spain and (b) the northern Apennine Mountains, Italy. Elevation data from GEBCO 30sec data. https://www.gebco.net/data_and_products/gridded_bathymetry_data/

Figure 2. Geodetic, paleogeodetic, and earthquake focal mechanism data from southern Spain. Generalized geology (from Azañon et al., 2015), focal mechanism solutions for normal faults (from Mancilla et al, 2013), mineral lineations [short red lines] (from Martinez-Martinez et al., 2002), results from 10-years of observed velocity GPS permanent [black arrows, with uncertainties] (from Gutscher et al., 2012), and campaign [yellow arrows and uncertainties] (from Koulali et al., 2011), stations in an African (Nubia) fixed reference frame. SN = Sierra Nevada. Bathymetry color depths as in Fig. 1. Elevation data from 30 m SRTM NASA JPL. NASA Shuttle Radar Topography Mission Combined Image Data Set. 2014, distributed by NASA EOSDIS Land Processes DAAC, https://doi.org/10.5067/MEaSUREs/SRTM/SRTMIMGM.003.

Figure 3. Simplified geologic map showing sample sites around the Sierra Nevada massif, southern Spain. Litho-structural map of the study area (modified from Azañon et al., 2015). Nevado Filabride complex: (1) Ragua unit, (2) and (3) Calar–Alto unit, Palaeozoic and Permo–Triassic rocks, respectively, and (4) Bédar–Macael unit. Alpujarride complex: (5) Lújar–Gador unit and (6) upper Alpujárride units. Malaguide complex: (7) undifferentiated. Neogene sediments: (8) Miocene and (9) Pliocene to Quaternary. 10) Low-angle inactive normal fault, 11) high angle normal fault, 12) high angle normal fault (undifferentiated), 13) strike-slip fault, 14) anticline, and 15 syncline. Gdb: Guadix basin and Grb: Granada basin. Lower hemisphere stereographic projection of AMS determined principal axes, k_1-red squares, k_2, green triangles, k_3, blue circles. Bedding orientation shown along with axes orientation uncertainties. Elevation data from 30 m SRTM NASA JPL. NASA Shuttle Radar Topography Mission Combined Image Data Set.

2014, distributed by NASA EOSDIS Land Processes DAAC, https://doi.org/10.5067/MEaSUREs/SRTM/SRTMIMGM.003.

Figure 4. Examples of specimen collection from poorly cemented samples. (a) a sampling surface is carved in a massive sandstone of the upper Miocene Laga Fm., northern Apennines (b) the same is done on a subhorizontal layer of a poorly cemented, fine calcareous sandstone from an upper Middle Pleistocene fluvial terrace exposed in a wine cellar at the Geological Observatory of Coldigioco, northern Apennines. Both samples were hardened with a dilute sodium silicate solution. Three to four oriented blocks were collected from each sampling site. Samples were oriented with a Brunton compass and located with a handheld GPS receiver, labeled, and photographed.

Figure 5. Magnetic mineralogy of Sierra Nevada specimens. (top) Low temperature (MS vs T) measured on a KLY-3s Kappabridge at Lehigh University. Data in red and paramagnetic modeling in green indicating the proportion of the magnetic susceptibility carried by paramagnetic grains. Results from all measurements indicate that the magnetic susceptibility of the Spanish samples varies from being dominated by paramagnetic to ferromagnetic mineral grains. The kinematic interpretation is the same in all cases. (bottom) High temperature (MS vs T) measurements showing heating from room temperature (20˚C) to 700˚C and subsequent cooling back to room temperature. All four plots show evidence of the ferromagnetic mineral magnetite (Curie Temperature of 580˚C). A lower temperature phase is indicated in site 3, possibly maghemite. Site 6 shows the formation of additional magnetite during heating because of the much stronger susceptibility upon cooling. Heating curves are in red and cooling curves in blue.

Commented [MOU5]: Please provide details for how this was performed. I'm assuming a Curie-Weiss relationship was fitted to the data: if so, could you specify the formula and constants used?

Commented [MOU6]:

Figure 6. (a) Plot of mean susceptibility (K_m) with respect to ellipsoid shape, (T) for Sierra Nevada samples. Oblate shapes are positive T whereas prolate shapes are negative T. The specimens are color coded by site and consistent with Fig. 3. The lack of correlation between ellipsoid shape and susceptibility strengthen the conclusions based on the site comparisons we present here. (b) Jelinek diagram of Sierra Nevada specimens colored by site and consistent with Fig. 3. All AMS measurement have a low anisotropy (less than 12% Pj,) and nearly all specimens are oblate (T>0). T and Pj are calculated as follows: if n1=ln(t1), n2=ln(t2), n3=ln(t3),where t1, t2, and t3 are the eigenvalues, then T=(2n2-n1-n3)/(n1-n3) and P'=exp(sqrt(2[(n1-nmean)2 + (n2-nmean)2 + (n3-nmean)2]) and nmean=(n1+n2+n3)/3 (Jelinek, 1981).

Figure 7. All Sierra Nevada massif AMS data. Lower hemisphere, stereographic projection of the principal axes of susceptibility orientations for all specimens determined from AMS measurements in stratigraphic coordinates (Fig. 3). Arrows outside the stereonet periphery are parallel to the mean long axis (k_1) orientation. *k_1= Maximum axis, k_2= intermediate axis, k_3= minimum axis.*

Figure 8. Kinematic summary of AMS Example I. Comparison of paleogeodetic methods around the Sierra Nevada massif, Spain illustrating the validity of AMS determined principal extension direction (k_1).

Figure 9. (a) Location map showing the topography, major known faults with black lines, the location of large, historic earthquakes in orange circles (from Boncio et al., 1998), the drainage divide as a red line, and GPS geodetic velocities with uncertainties in red arrows (from Hreinsdottir and Bennett, 2009) in the northern Apennine showing our research corridor (gray shaded box). Elevation data from TINITALY 10 m DEM (Tarquini et al., 2012). Alto Tiberina Fault (ATF), Ancona (A), Apiro (Ap), Arezzo (Ar), Ascoli Piceno (AP), Cagli (C), Camerino (Cm), Cascia (Ca), Fabriano (F), Foligno (Fo), Gola di Frasassi (GdiF), Gubbio (G), Jesi (J), Macerata (M), Norcia (N), Osservatorio Geologico Coldigioco (OGC), Perugia (P), Spoleto (S), Visso (V). (b) Inset regional map showing the plate boundary and location of Fig 9a. (c) Synthetic cross section of the region in (a) projected to the X-X' line (modified from Chiaraluce et al., 2017). Normal faults in black, thrust faults in red, top of Permo-Triassic evaporites in blue, top of carbonates in green. (d) Photo of an exposed bedrock fault scarp from the Umbrian Apennines. Fault scarps are uncommon in most of Marche.

Figure 10. Results of AMS analysis in the northern Apennines over 1:10,000 simplified geology (from regione Marche and Umbria, regione.marche.it; http://dati.umbria.it/) and topography. Elevation data from 30 m NASA JPL. NASA Shuttle Radar Topography Mission Combined Image Data Set. 2014, distributed by NASA EOSDIS Land Processes DAAC, https://doi.org/10.5067/MEaSUREs/SRTM/SRTMIMGM.003. Extensional earthquake epicenters compiled from Rovida et al. (2020). The presence of a tectonic fabric was determined by clustering of k_1 declinations outside of the expected compaction fabric. Axis certainty represents the percentage of specimens of the total used to calculate a mean k_1 vector. Right Legend: 1. Holocene fill; 2. 1st order Quaternary Terrace (Qt1); 3. 2nd order Quaternary Terrace (Qt2); 4 3rd order Quaternary Terrace (Qt3); 5. Argille Azzurre Fm; 6. Scaglia Rossa Fm; 7. Maiolica Fm; 8. Bisciaro Fm; 9. Thrust fault trace; 10. Normal fault trace; 11. Alto-Tiberina detachment; 12. Drainage divide; 13. Large historic, but pre-instrument earthquakes of unknown origin (see Fig. 9).

Figure 11. (a) Hysteresis curves for representative samples of the studied Apennine Range geologic formations (see location in Fig. 10). Paramagnetic susceptibility clearly dominates all the specimens as revealed by the slope of the loops. (b) Example of a specimen where the paramagnetic contribution has been removed in order to enhance the ferromagnetic contribution (loop in black). (c) Example of a specimen where diamagnetism dominates the total magnetic susceptibility.

Figure 12. Lower hemisphere stereographic projection of representative sites showing representative fabric patterns in Quaternary deposits (a) and older rocks in the Apennine foreland (b), (c), and older rocks south of the extensional front (d). The orientation of bedding is shown when not horizontal.

Figure 13. (a) Plot of mean susceptibility (K_m) with respect to degree of anisotropy, (P_j) for the Apennine specimens. The specimens are color coded by site. (b) Jelinek diagram of Apennine specimens, colored by site. All AMS measurements are consistent with low strains (Pj, degree of anisotropy) and nearly all specimens are oblate (T>0).

808

Table A1.

Sample	Lat	Long	Elevation (m)	Formation	Age	Composition and Texture
Spain						
SN1	37.04972	-3.64923	853	-	Quaternary	Siliciclastic silt
SN3	36.9539	-3.05758	555	-	Quaternary	Siliciclastic silt
SN4	36.95832	-2.99537	600	-	Neogene	Siliciclastic silt
SN5	37.26138	-3.73503	609	-	Neogene	Siliciclastic silt
SN6	37.00809	-2.56091	501	-	Neogene	Siliciclastic sand
SN7	37.22960	-3.11414	1037	-	Neogene	Siliciclastic sand
Italy						
AP1	43.34778	13.12132	462	Ghiaia Urbisaglia Fm	Early Pleistocene	Calcareous and siliciclastic silt
AP2	43.36193	13.09481	454	Bisciaro Fm	Early Miocene	Argillaceous marl
AP3	43.35226	13.11542	502	Laga Fm	Late Miocene	Argillaceous silty sand
AP4	43.42590	13.23293	217	Qt4 alluvium	Late Pleistocene	Calcareous and siliciclastic silt
AP5	43.46141	13.30483	126	Argille Azzurre Fm	Pliocene	Siliciclastic blue-gray silty clay
AP6	43.53607	13.59282	218	Scaglia Variegata Fm	Late Eocene	Argillaceous marl
AP7	43.55456	13.57438	215	Bisciaro Fm	Early Miocene	Argillaceous marl
AP8	43.40956	13.10795	425	Argille Azzurre Fm	Pliocene	Siliciclastic blue-gray silty clay
AP9	43.30225	13.02115	469	Fm Camerino (Laga Fm)	Late Miocene	Siliciclastic argillaceous sandy silt
AP10	43.40180	12.96773	223	Qt3 alluvium	Middle Pleistocene	Calcareous and siliciclastic silt
AP11	43.41049	12.58075	553	Marnosa Arenacea Fm	Middle Miocene	Siliciclastic argillaceous sandy silt
AP12	43.38627	12.56814	638	Marnosa Arenacea Fm	Middle Miocene	Siliciclastic argillaceous sandy silt
AP13	43.38261	12.56343	629	Bisciaro Fm	Early Miocene	Argillaceous marl
AP14	43.20721	13.00143	520	Scaglia Cinerea Fm	Oligocene	Siliciclastic and calcaerous argillaceous sandy silt
AP15	43.24922	12.97616	406	Scaglia Cinerea Fm	Oligocene	Siliciclastic and calcaerous argillaceous sandy silt
AP16	43.51872	12.72748	500	Scaglia Cinerea Fm	Oligocene	Siliciclastic and calcaerous argillaceous sandy silt
AP17	43.56574	12.80247	421	Laga Fm	Late Miocene	Siliciclastic argillaceous sandy silt

809
810
811

812
813

Figure 1

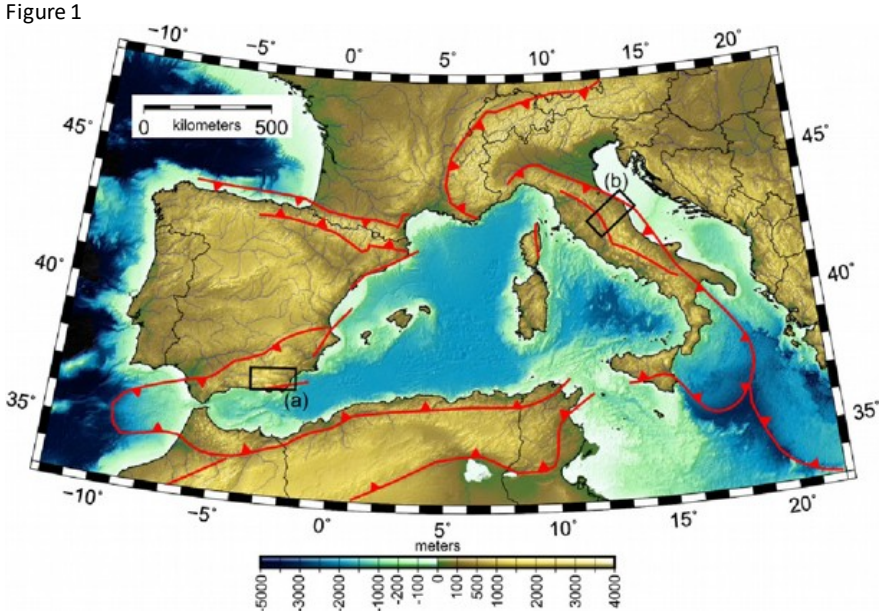

814
815

Figure 2

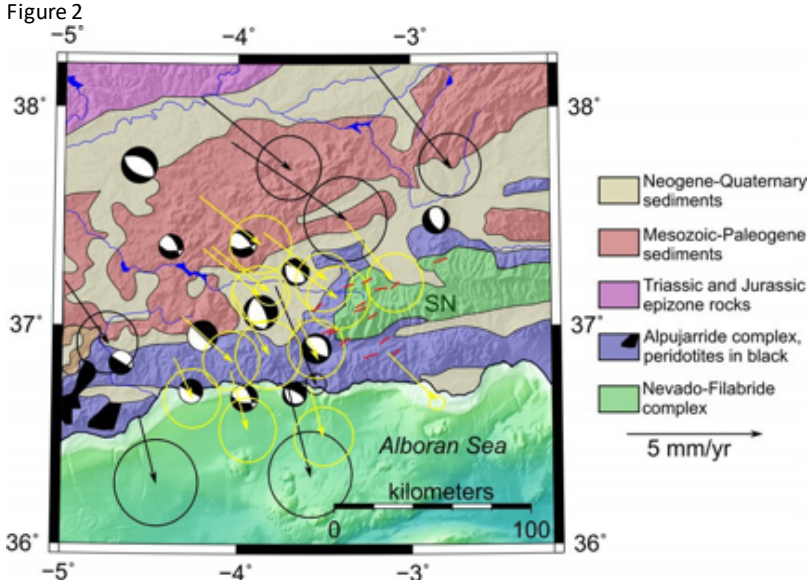

816
817

818 Figure 3

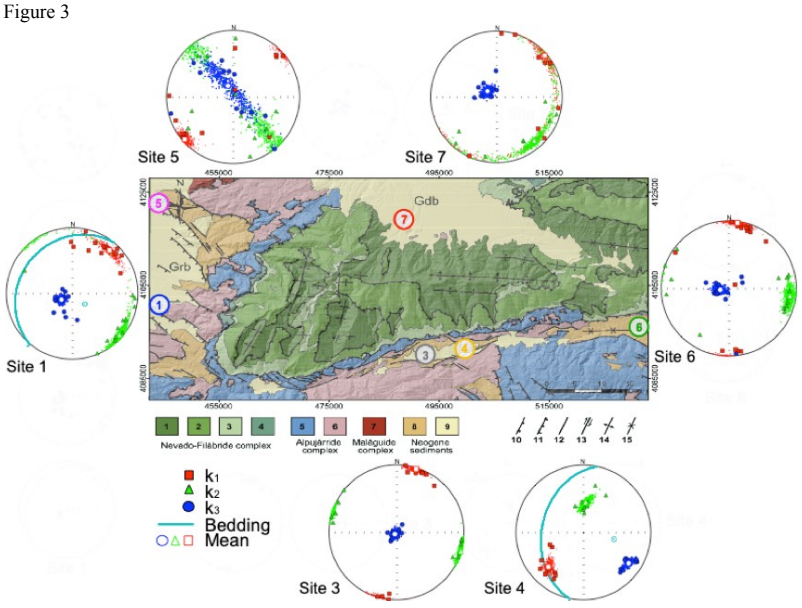

819
820
821
822
823
824
825
826
827

Figure 4

828
829
830
831

Figure 5

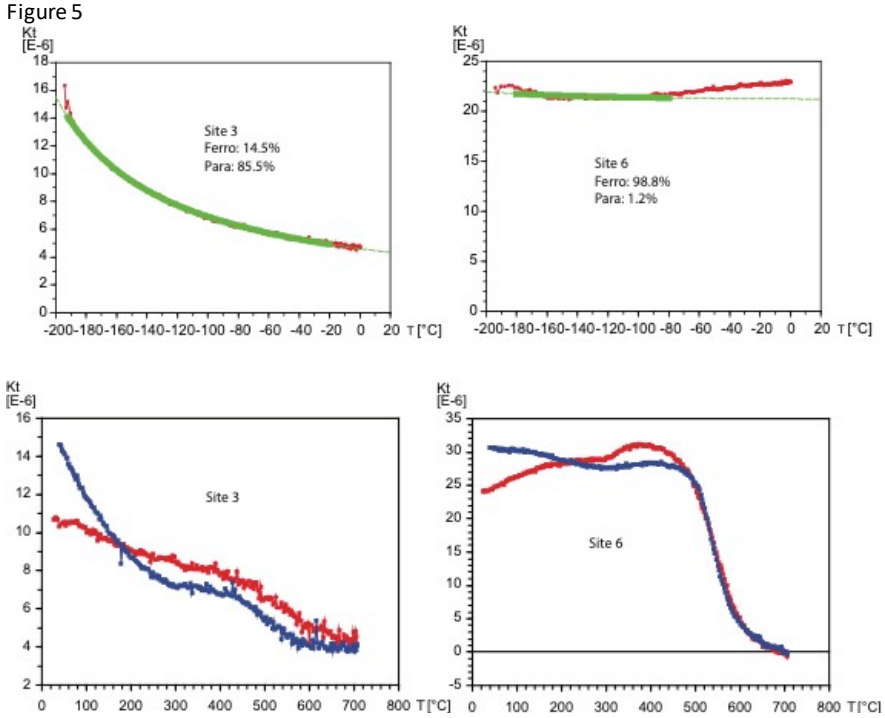

832
833
834

Figure 6

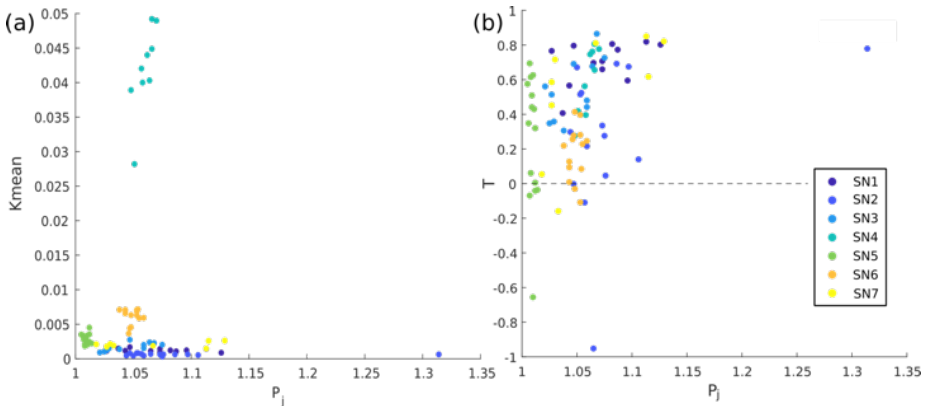

839 Figure 7
840
841

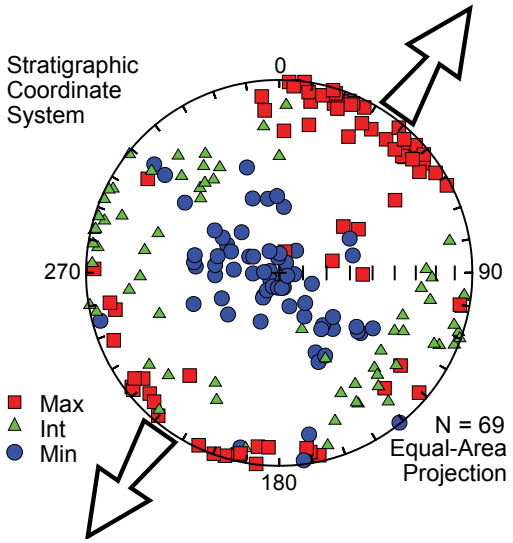

842

Figure 8

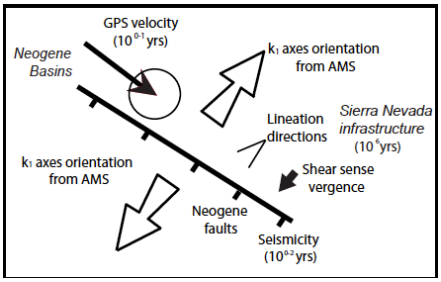
GPS velocity
(10^{0-1} yrs)
Neogene
Basins
k_1 axes orientation
from AMS
Lineation
directions
Sierra Nevada
infrastructure
(10^{6}yrs)
k_1 axes orientation
from AMS
Shear sense
vergence
Neogene
faults
Seismicity
(10^{0-2} yrs)

Figure 9

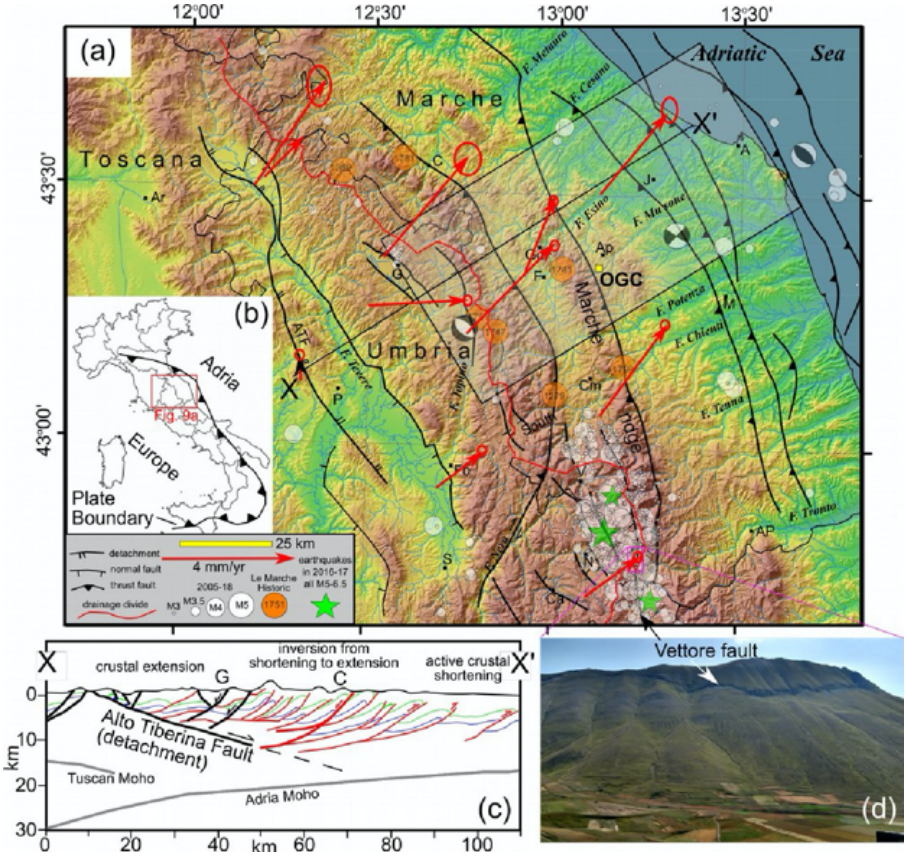
12°00'
12°30'
13°00'
13°30'
43°30'
43°00'
(a)
Adriatic Sea
Marche
Toscana
Umbria
OGC
(b)
Adria
Europe
Plate Boundary
Fig. 9a
25 km
4 mm/yr
detachment
normal fault
thrust fault
drainage divide
earthquakes in 2016-17 all M5-6.5
2005-18
Le Marche Historic
M3
M3.5
M4
M5
1751
X
X'
crustal extension
inversion from shortening to extension
active crustal shortening
Alto Tiberina Fault (detachment)
Tuscan Moho
Adria Moho
km
0
10
20
30
0
20
40
60
80
100
(c)
Vettore fault
(d)

Figure 10

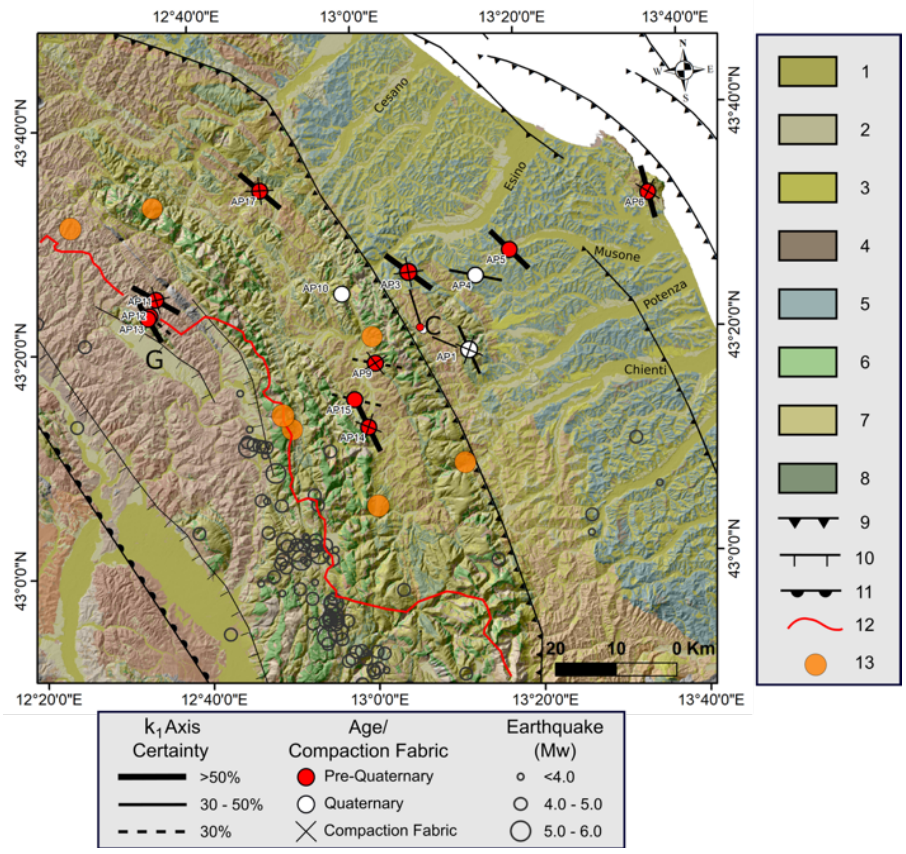
12°40'0"E
13°0'0"E
13°20'0"E
13°40'0"E
43°40'0"N
43°20'0"N
43°0'0"N
Cesano
Esino
Musone
Potenza
Chienti
AP1
AP2
AP3
AP4
AP5
AP6
AP7
AP8
AP9
AP10
AP11
AP12
AP13
AP14
AP15
G
C
20
10
0 Km
1
2
3
4
5
6
7
8
9
10
11
12
13
k1 Axis Certainty
>50%
30 - 50%
30%
Age/ Compaction Fabric
Pre-Quaternary
Quaternary
Compaction Fabric
Earthquake (Mw)
<4.0
4.0 - 5.0
5.0 - 6.0

Figure 11

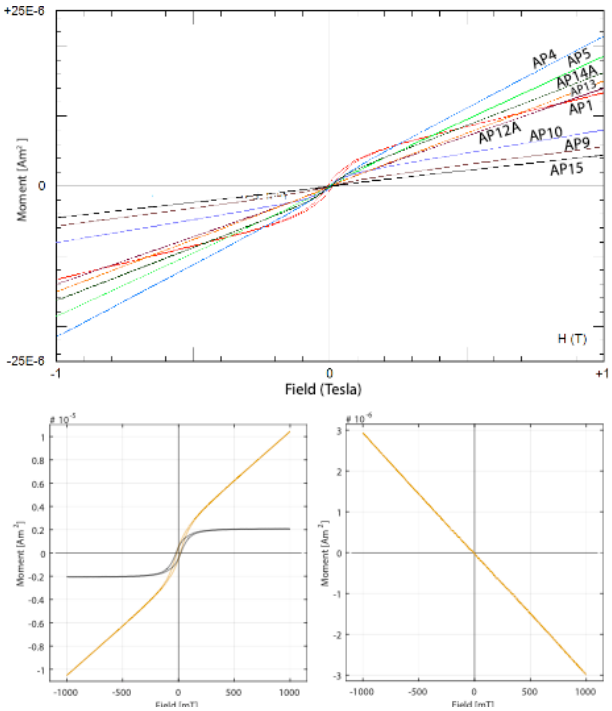

858
859
860

Figure 12

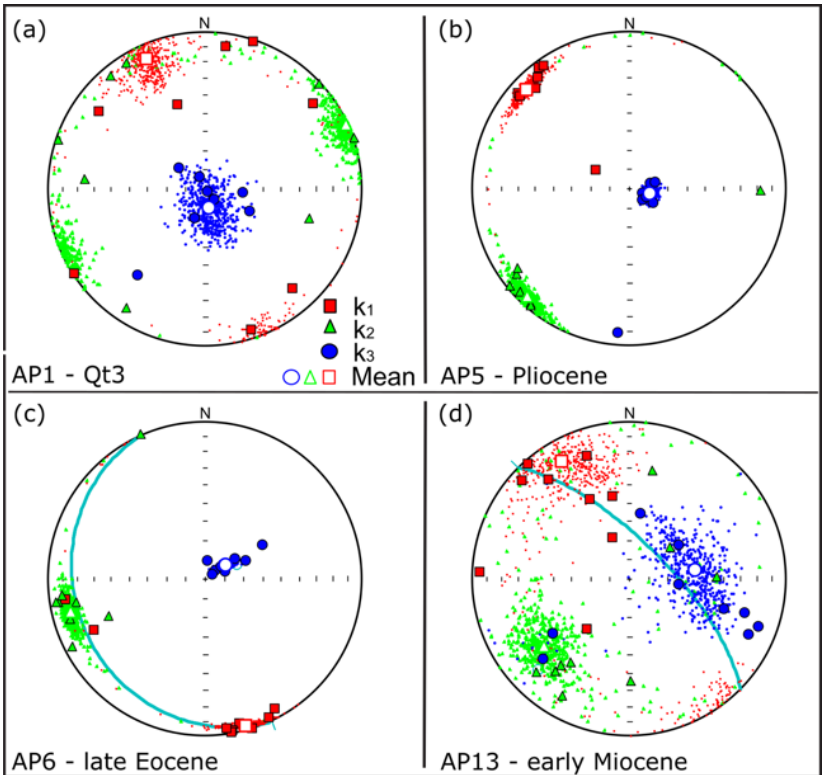
(a)
N
k1
k2
k3
Mean
AP1 - Qt3
(b)
N
AP5 - Pliocene
(c)
N
AP6 - late Eocene
(d)
N
AP13 - early Miocene

Figure 13

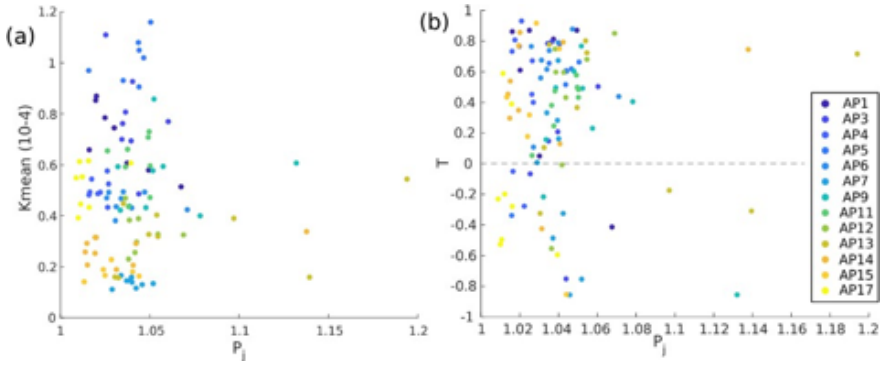
(a)
Kmean (10-4)
P_j
(b)
T
P_j
AP1
AP3
AP4
AP5
AP6
AP7
AP9
AP11
AP12
AP13
AP14
AP15
AP17